Research Article | Vol. 27, No. 5 | 4 Mar 2019 | OPTICS EXPRESS 7537
Optics EXPRESS

Suppression of reflected side lobes in narrow-band X-ray multilayer coatings

YOUWEI YAO[1,2,*] AND HIDEYO KUNIEDA[1]

[1] *Department of Physics, Nagoya University, Furo-cho, Chikusa-ku, Nagoya, Aichi 464-8602, Japan*
[2] *Space Nanotechnology Laboratory, MIT Kavli Institute for Astrophysics and Space Research, Cambridge, MA 02139, USA*
*yao.xray@gmail.com

Abstract: We present an analytical method for the design of narrow-band X-ray multilayer coatings having greatly reduced reflected side-lobe intensity, for the realization of X-ray mirrors that have improved spectral purity. The method uses a specific variation of the individual layer thicknesses as a function of depth in the multilayer stack, derived from Laplace transform analysis of the multilayer's reflectance profile. The design process and mathematical foundations are outlined. Pt/C multilayers with 5 nm *d*-spacing for hard X-rays are designed, fabricated and measured to demonstrate the validity and effectiveness of the method are presented. As an extrapolation, three additional side lobe suppressed multilayers for soft X-rays and EUVs are also designed and investigated: 1) Cr/Sc multilayer for soft X-rays (4.96 nm wavelength) at high grazing angle (30°), 2) Mo/Si multilayer for EUV (13.5 nm wavelength) at normal incidence angle and 3) SiC/Mg multilayer for EUV (30.4 nm wavelength) at normal incidence angle. The calculated reflectances demonstrate that the presented method is robust for the energy range from X-rays to EUVs.

1. Introduction

Nanometer-scale multilayer structures are now widely used as X-ray reflective coatings for a variety of applications [1–4]. Periodic multilayer coatings in particular, which consist of a number of repeating, identical bi-layers, can act as highly efficient narrow-band X-ray filters operating in reflection. Periodic multilayer coatings have thus found wide application as monochromators for use with synchrotron radiation and other high-intensity light sources [4–6]. Multilayer-coated mirrors typically provide a somewhat wider spectral band-pass relative to single-crystal monochromators [7], and can thus deliver higher photon flux at the expense of reduced spectral resolution. However, the side lobes (or so-called Kiessig fringes [8]) that are present in multilayer reflectance profiles can degrade spectral purity. The focus of this work is the suppression of reflected spectral side lobes in narrow-band X-ray multilayer coatings.

Side lobes in multilayer coatings designed for operation in the visible portion of the spectrum have been suppressed previously by precisely controlling the thickness and the optical constants of the materials comprising each layer in the film stack, using, e.g., chemical etch-leach or co-evaporation processes [9–12]. This approach cannot be used effectively for X-ray multilayers, however, due to the nature of optical constants of solids in the X-ray range, and incompatibility with the deposition techniques required for precise X-ray multilayer deposition [1]. Aperiodic coatings, comprising a stack of non-repeating bi-layers that are described numerically, rather than parametrically, offer another promising method for side-lobe suppression. The design of such coatings amounts to a reverse optimization problem, where the thicknesses of the individual layers in the multilayer stack are treated as independently adjustable parameters, and are then varied, following a figure-of-merit minimization procedure, in order to match a target reflectance function, as described, for example, by Kozhevnikov [13]. In this paper we present a new approach for side-lobe

#347799 https://doi.org/10.1364/OE.27.007537
Journal © 2019 Received 12 Oct 2018; revised 28 Nov 2018; accepted 23 Dec 2018; published 28 Feb 2019

Optics EXPRESS

suppression, based on control of individual layer thicknesses following purely analytical methods.

2. Theory

The condition for constructive interference in a periodic multilayer is described (approximately) by Bragg's law, $n\lambda = 2d\cdot\sin(\theta)$, where n is the Bragg order, d is the multilayer d-spacing or bi-layer thickness, θ is the grazing incidence angle and λ is the photon wavelength. Kozhevnikov's analytical work has been proved to be very useful for depth-graded multilayer design, however, not valid for stationary structure (periodic multilayer). We have previously simplified Kozhevnikov's theory for the design of a periodic multilayers [14] in order to analyze the reflectance profiles of block-structure "supermirror" coatings used for X-ray telescopes. In the specific case of an electro-magnetic wave propagating in a multilayer structure where we can assume that the reflection coefficient r<<1 at each interface in the film stack (a generally valid assumption in the X-ray region), the complex reflection amplitude $r(\kappa)$ is given by:

$$\begin{gathered} r(\kappa) = \frac{jk^2}{4\kappa}\sum_{n=1}^{\infty} B_n \exp(-j\pi n\Gamma) \times \mathcal{L}\{\exp[-j2\pi n y(z)]\,|_0^L\} + S_-(0) \\ \kappa = k\sqrt{\mu - \cos^2(\theta)}, \mu = \Gamma\varepsilon_1 + (1-\Gamma)\varepsilon_2 \\ B_n = 2(\varepsilon_1 - \varepsilon_2)\frac{\sin(\pi n\Gamma)}{n\pi}, y(z) = z/d \end{gathered} \tag{1}$$

where ε_1 and ε_2 correspond to the dielectric constants of the two materials that make up each bi-layer, μ is the mean dielectric constant, $k = 2\pi/\lambda$ is the wave number in vacuum, κ is the surface-normal component of the complex wave vector propagating in the multilayer structure, $d = d_1 + d_2$ is the bi-layer thickness, L is the total film thickness, the notation $|_0^L$ means the exponential function on its left side is within the domain $(0,L)$, $\Gamma = d_1/(d_1 + d_2)$ is the relative layer thickness ratio of each bi-layer, $y(z) = z/d$ is a continuous function of depth z in each layer, and L signifies the Laplace transform. The term $S_-(0)$ is originated from a high order harmonic in the spectrum of multilayer's dielectric function, which is negligible around the first order Bragg peak, as has been demonstrated in [14]. The multilayer reflectance profile is given by $R = |r(\kappa)|^2$. We define the exponential term $\exp[-j2\pi n y(z)]|_0^L$ as the multilayer's "Structure Function"; and define in turn the Laplace transform of the Structure Function $L\{\exp[-j2\pi n y(z)]|_0^L\}$ as the multilayer's "Spectral Function":

$$\mathcal{L}\{\exp[-j2\pi n y(z)]\,|_0^L\} = \frac{1}{j(2\kappa - nk_0)}[1 - \exp(-L2\kappa j)] \tag{2}$$

where $k_0 = 2\pi/d$. In this work we retain only the $n = 1$ term, because the bandwidth near the 1st order Bragg peak is the most important parameter for most applications, and furthermore the reflectance profile near the 1st order Bragg peak, i.e., $\kappa \approx k_0/2$, is dominated by the first term in the series. In the case of a periodic multilayer, where each bi-layer is identical and Γ is thus constant with depth in the film, the Structure Function is thus multiplied by a boxcar window function of width L; this is the source of the side lobes in the resulting Spectral Function, and thus in the multilayer's reflectance profile. For the plot of the Spectral Function and its correlation with reflectance, please see Fig. 8 in [14].

In order to suppress the side lobes that are otherwise present in periodic multilayers, the boxcar window function just explained can be replaced with a Gaussian window function [15]. This can be achieved by using a specific variation in Γ with depth in the multilayer stack. (The mean dielectric constant μ will thus vary with depth in the film as well in that case. However, as the refractive index is very close to 1 in the X-ray region for all materials, we approximate μ as constant with depth and ignore this small effect.) The exponential term

Optics EXPRESS

B_1exp(-$j\pi\Gamma$) in Eq. (1) is rearranged and placed in front of the periodic exponential term (exp[-$j2\pi y(z)$]) as follows,

$$r(\kappa)=\frac{jk^2(\varepsilon_1-\varepsilon_2)}{2\pi\kappa}\mathcal{L}\{\sin[\pi\Gamma(z)]\times\exp[-j\frac{2\pi}{d}z-j\pi\Gamma(z)]\,|_0^L\}\tag{3}$$

The term sin[$\pi\Gamma(z)$] thus provides the needed Gaussian window function. However, the layer thickness ratio Γ is not continuous, but is a discrete function of depth. We therefore use instead the discrete window function:

$$\sin[\pi\Gamma(m)]=\exp[-\frac{1}{2}(\frac{m-(N-1)/2}{\sigma(N-1)/2})^2]\tag{4}$$

where m = 1, 2, … is the index of each bi-layer, with the m = 1 bi-layer located at the surface of the film, and N is the total number of bi-layers. The discrete window function sin[$\pi\Gamma(m)$] thus follows a Gaussian distribution, and we define σ as its standard deviation. For example, σ = ∞ corresponds to a periodic multilayer with Γ = 1/2, which produces the boxcar window already discussed. If σ is near 1, then Γ will vary relatively slowly within its allowable range of 0 to 1. If σ is too close to 0, however, then Γ will vary more rapidly than can be realized in practice. In any case, the variation in Γ adds an offset to the d-spacing of the exponential term in Eq. (3). However, because Γ is small compared with the term $2z/d$, and because it can be made to vary nearly linearly with bi-layer number (as discussed further below in section 3), this offset can be ignored.

3. Design examples

To apply the theory just outlined, the values of three parameters – d, N, and σ– must be determined in order to effectively suppress side lobes in a narrow-band multilayer that is designed to operate at a specific incidence angle and photon wavelength. We use Parratt's algorithm [16] to precisely calculate the reflectance of candidate multilayer structures. The multilayer d-spacing is determined through reflectance simulations using the required incidence angle and the target photon wavelength. The optimum number of bi-layers N is determined by increasing N until "saturation" is reached, i.e., the point at which the magnitude of 1st order Bragg peak cannot be increased further through the addition of more bi-layers [17]. Once d and N are specified, an optimum value for the width of the Gaussian window function σ can be determined, based on the observed side lobe suppression. Smaller σ values lead to greater side lobe suppression, however a value for σ that is too small can lead to Γ values that are too close to 0 or 1 at the boundary of the structure; in that case the design would require layers that are too thin to fabricate in practice. For example, base on our ability on Pt/C multilayer deposition (DC magnetron sputtering) [18], the smallest achievable layer thickness is ~0.6 nm, so a value of σ ~0.7 is optimal.

The solution of Eq. (4) for $\Gamma(m)$ can be monotonically increasing, monotonically decreasing or oscillating, between the allowable range of 0<Γ<1. In this work, the variation in Γ was constrained to be monotonic, for the following reasons: first, accurate layer thicknesses can be more easily realized when the layer thickness variation in the stack varies slowly; second, the critical angle for total external reflection can be reduced by properly adjusting the layer thickness ratio near the top of the film stack, thereby increasing spectral purity in some applications; and third, the use of a $\Gamma(m)$ function that is close to linear will lead to only a minimal d-spacing offset in the exponential term in Eq. (3), thereby avoiding any significant broadening of the Bragg peak.

3.1 Side lobe suppressed multilayers for hard X-rays

Several candidate multilayer structures have been designed for θ = 0.7° and λ = 0.1 nm. We selected platinum and carbon as the combination since its available in our lab [18]. The multilayer d-spacing was fixed at $d = 5$ nm in all cases. Coatings with either $N = 20$ or $N = 30$ bi-layers were compared, and σ values of 0.7, 1.0, and ∞ were investigated. The calculated reflectance-vs.-energy profiles from all designs studied are shown in Fig. 1. The structure of one particular multilayer, in this case having $N = 30$ and $\sigma = 0.7$, is shown in Fig. 2. The individual C and Pt layer thicknesses are shown as red circles and blue squares, respectively. The individual layer thicknesses vary slowly with bi-layer index. The discrete Gaussian window function [Eq. (4)] is plotted using green crosses in Fig. 2.

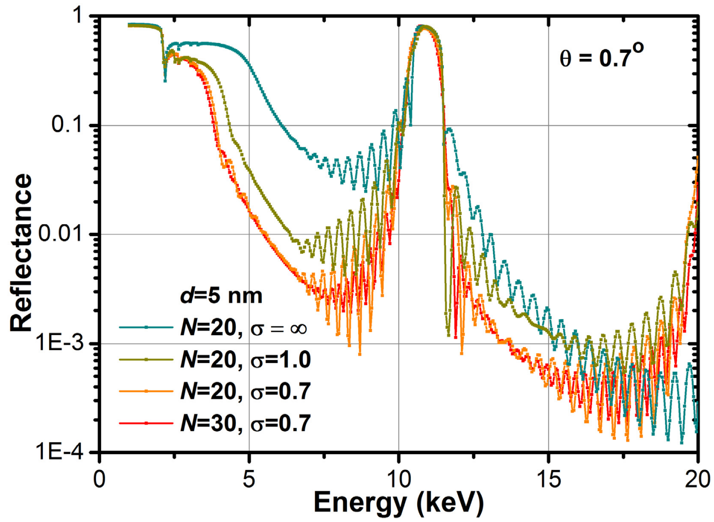

Fig. 1. Calculated reflectance-vs.-energy profiles of narrow-band Pt/C hard X-ray multilayers. Reflectance is calculated using Parratt's algorithm. Side lobes are significantly suppressed when σ is equal to 0.7 or 1.0. While the 1st order peak reflectance saturates at $N = 20$, better side-lobe suppression in fact can be realized using $N = 30$ bi-layers.

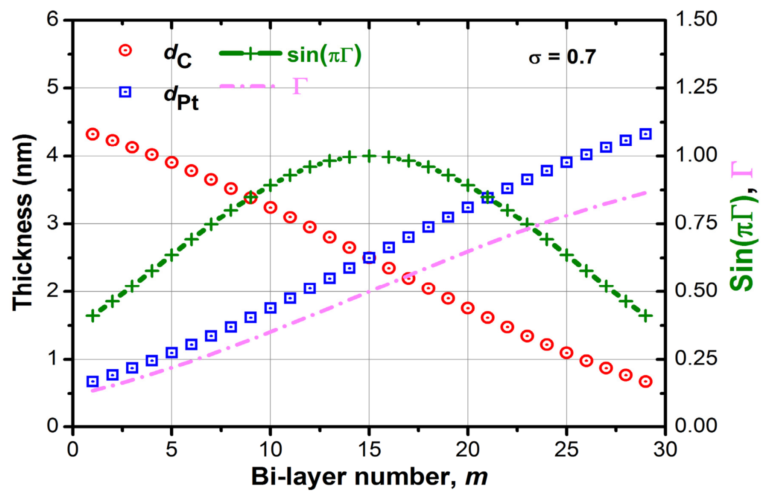

Fig. 2. Layer thickness distributions (red circles for C, blue squares for Pt) and the Gaussian window function (green crosses) of a multilayer structure having $d = 5$ nm, $N = 30$ and $\sigma = 0.7$. The corresponding reflectance-vs.-energy profile is shown as the red line in Fig. 1. Bi-layer number $m = 1$ is located at the surface of the film.

As is evident from Fig. 1, a significant reduction in side-lobe intensity near the 1st order Bragg peak can be achieved when the thickness ratio $\Gamma(m)$ follows the distribution derived from Eq. (4). Better side-lobe suppression is observed for $\sigma = 0.7$ relative to $\sigma = 1.0$.

Optics EXPRESS

Furthermore, better side-lobe suppression is found using N = 30 bi-layers, even though the intensity of the 1st order Bragg peak saturates with N = 20 bi-layers.

It is also apparent from Fig. 1 that the reflection intensity near the 2nd order Bragg peak is higher for the films having σ values of 0.7 or 1.0 relative to the case of σ = ∞ (i.e., a conventional periodic multilayer). In the case of a periodic multilayer with Γ = 0.5, the 2nd order peak is completely suppressed due to destructive interference. However, for the films where Γ varies with bi-layer number (i.e., σ = 0.7 or 1.0), the condition for destructive interference is no longer satisfied near the 2nd order Bragg peak. This leads in turn to increased reflected intensity near 2nd order; there is also a slight broadening of the 1st order peak.

3.2 Side lobe suppressed multilayers for soft X-rays and EUVs

As an extrapolation, the analytical method has also been attempted on soft X-ray and EUV multilayer structures. In these wavebands the refractive index of materials are more variable. Variation of Γ leads to variation of the mean refractive index within each layer pair, and therefore to changes of the optical path, breaking the Bragg condition and broadening the Bragg peak. To solve this problem, the d-spacing of each bi-layer is adjusted by multiplying a factor,

$$d_m = d_{\sigma=\infty} \cdot \frac{0.5 \cdot (\mathrm{Re}(\sqrt{\varepsilon_1 - \cos^2(\theta)}) + \mathrm{Re}(\sqrt{\varepsilon_2 - \cos^2(\theta)}))}{\Gamma(m) \cdot \mathrm{Re}(\sqrt{\varepsilon_1 - \cos^2(\theta)}) + (1-\Gamma(m)) \cdot \mathrm{Re}(\sqrt{\varepsilon_2 - \cos^2(\theta)})} \tag{5}$$

where d_m is the d-spacing of m-th layer pair from the top, $d_{\sigma=\infty}$ means the d-spacing of a standard multilayer, ε_1 and ε_2 are dielectric constants which are equal to the square of the complex refractive index, and θ is the grazing angle of the incident photon. The notation Re means the real part of the complex number.

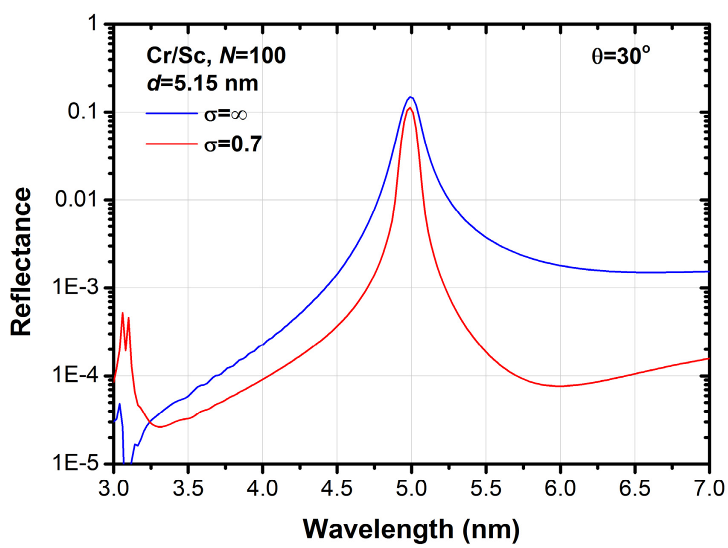

Fig. 3. Calculated reflectance-vs.-wavelength profiles of narrow-band Cr/Sc soft X-ray multilayers. Reflectance is calculated using Parratt's algorithm. The target center wavelength is 4.96 nm (250 eV). The peak reflectivity of the standard multilayer is 14.9%, while that of the side lobe suppressed multilayer is 11.3%. Side lobes are significantly suppressed when σ is equal to 0.7.

Optics EXPRESS

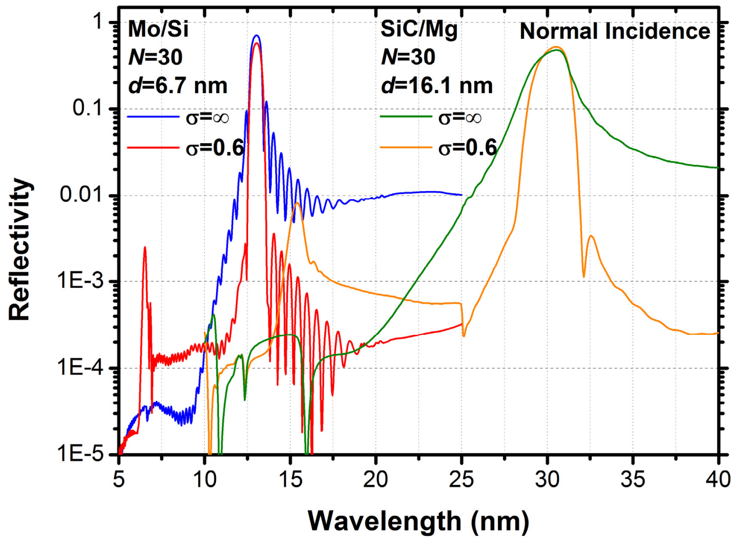

Fig. 4. Calculated reflectance-vs.-wavelength profiles of narrow-band Mo/Si and SiC/Mg EUV multilayers at normal incidence angle (90°). Side lobes are significantly suppressed when σ is equal to 0.6. Peak reflectivity of 1) blue line: 71.0%, 2) red line: 57.8%, 3) green line: 48.1%, and 4) orange line: 52.3%.

By using Eqs. (4) and (5), different types of side lobe suppressed multilayers have been designed for soft X-rays and EUVs. The calculated reflectance for wavelengths are shown in Figs. 3 and 4.

Figure 3 shows the results for the soft X-ray multilayer Cr/Sc with 100 layer pairs, which is typical [19]. The grazing incident angle is 30° and the *d*-spacing, $d_{\sigma=\infty}$, is set at 5.15 nm so the center wavelength of the Bragg peak is 4.96 nm (250 eV). Popular EUV multilayers are Mo/Si and SiC/Mg for 13.5 nm and 30.4 nm, respectively, which could be useful for lithography optics and astronomical applications [20].

Figure 4 shows results for Mo/Si and SiC/Mg designs. For Cr/Sc and Mo/Si side lobe suppressed multilayers, reflectivities at center wavelengths of the Bragg peaks are 5-15% lower than the standard multilayer; however, that of the SiC/Mg multilayer is higher than usual. On the other hand, the side lobe suppressed multilayer designs have much lower intensity at the waveband near first order Bragg peaks, which suggests that the design method is robust in those wave bands, and can significantly improve the signal-noise ratio for soft X-ray and EUV multilayers.

4. Experiment results

Based on our fabrication ability, two Pt/C multilayer coatings for hard X-ray reflection were deposited onto float glass substrates measuring 30 mm x 70 mm x 0.5 mm thickness, using a magnetron sputtering process described previously [18]. Both films had d = 5 nm *d*-spacing and $N = 30$ bi-layers; one film used $\sigma = \infty$ (i.e., a periodic multilayer with $\Gamma = 0.5$), the other $\sigma = 0.7$ for optimal side-lobe suppression. Reflectance-vs.-angle profiles at E = 8.05 keV were measured instead of reflectance-vs.-energy profiles due to two reasons: first, they are manifestation of the same phenomenon [21]; second, angular scan with a fixed X-ray energy is commonly available for most of the X-ray reflectometer systems which is convenient and high resolution (0.01°). The X-ray reflectometer is located at Ux lab in Nagoya University, which is a self-built 8-meter beam line. Cu-K_a line at 8.05 keV is generated by an X-ray generator, and then collimated by a DCM using Ge (111), attenuated by an aluminum foil, shaped by a 0.01mm wide and 2 mm high slit before being reflected by the sample mounted on a customized 6-axis translation stage. A proportional counter is used to measure the intensity of the reflected beam. The measurement results are shown in Fig. 5 along with calculated reflectance curves for each coating, computed using the Parratt's algorithm. The multilayer having σ = 0.7 has much lower reflected intensity than the standard coating on either side of the first order Bragg peak, i.e., within the angular ranges extending from ~0.3° to 0.8° and from ~1.2° to 1.4°. These results demonstrate the validity and effectiveness of the method described above.

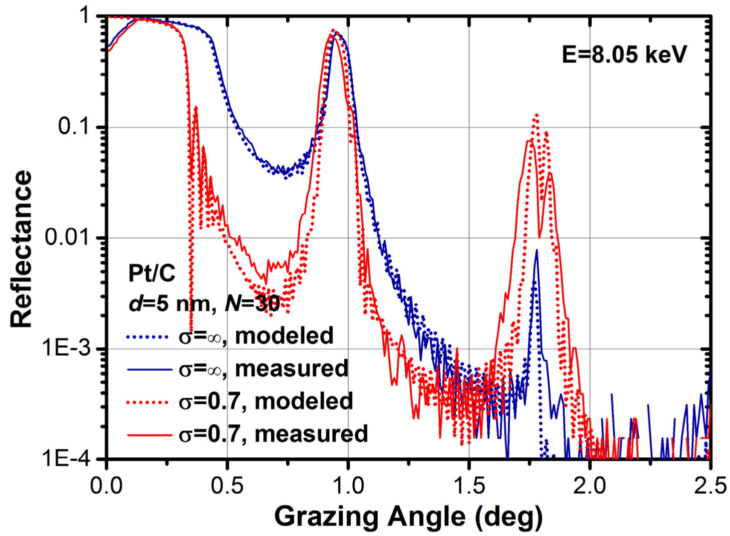

Fig. 5. Reflectance-vs.-angle profiles of both a standard periodic multilayer (blue) having Γ = 0.5 (σ = ∞), and a multilayer designed for optimal side-lobe suppression (red) using σ = 0.7. Measurements are shown as solid lines, modeled reflectance curves as dotted lines.

5. Conclusions

We have described a new analytical method for the design of narrow-band X-ray multilayers having greatly reduced side-lobe intensity. The method is based on the use of a precise variation in the layer thickness ratio Γ with depth in the multilayer stack, derived from Laplace transform analysis of the multilayer's reflectance profile. The magnitude of the side lobe suppression depends largely on just one parameter, the width (standard deviation) of the Gaussian window function that controls the variation in Γ. Using this method we have experimentally demonstrated a significant reduction of side lobe intensity in periodic Pt/C multilayers (d = 5 nm, N = 30) fabricated by magnetron sputtering. As an extrapolation, we also designed and investigated 1) Cr/Sc multilayer for soft X-rays (4.96 nm/250 eV) at high grazing angle (30°), 2) Mo/Si multilayer for EUV (13.5 nm wavelength) at normal incidence angle and 3) SiC/Mg multilayer for EUV (30.4 nm wavelength) at normal incidence angle to demonstrate the robustness of this method for energy range from X-rays to EUVs. Multilayer coatings fabricated following this approach can be used to achieve improved spectral purity in applications such as monochromators for high-intensity light sources and mirror coatings for X-ray/EUV optics image system.

Acknowledgments

The authors thank David Windt at Reflective X-ray Optics LLC and Mark Schattenburg at Space Nanotechnology Laboratory in MIT for useful discussions, suggestions and content editing. This work was completed in Ux Lab in Nagoya University in Japan.

References

1. D. Attwood and A. Sakdinawat, *X-rays and extreme ultraviolet radiation-principles and applications* (Cambridge University, 2016), Chap. 10.
2. K. S. Chon, Y. Namba, and K. H. Yoon, "Wolter type I x-ray focusing mirror using multilayer coatings," Appl. Opt. **45**(19), 4609–4616 (2006).
3. S. S. Panini, M. Nayak, K. C. S. Narendranath, P. C. Pradhan, P. S. Athiray, P. Sreekumar, G. S. Lodha, and M. K. Tiwari, "Development of multilayer mirrors for space-based astronomical x-ray optics," J. Opt. **47**(1), 91–95 (2018).
4. A. Sakdinawat and D. Attwood, "Nanoscale x-ray imaging," Nat. Photonics **4**(12), 840–848 (2010).
5. A. Rack, T. Weitkamp, M. Riotte, D. Grigoriev, T. Rack, L. Helfen, T. Baumbach, R. Dietsch, T. Holz, M. Krämer, F. Siewert, M. Meduna, P. Cloetens, and E. Ziegler, "Comparative study of multilayers used in monochromators for synchrotron-based coherent hard X-ray imaging," J. Synchrotron Radiat. **17**(4), 496–510 (2010).
6. G. Martínez-Criado, R. Tucoulou, P. Cloetens, P. Bleuet, S. Bohic, J. Cauzid, I. Kieffer, E. Kosior, S. Labouré, S. Petitgirard, A. Rack, J. A. Sans, J. Segura-Ruiz, H. Suhonen, J. Susini, and J. Villanova, "Status of the hard X-ray microprobe beamline ID22 of the European Synchrotron Radiation Facility," J. Synchrotron Radiat. **19**(Pt 1), 10–18 (2012).
7. D. Sokaras, T. C. Weng, D. Nordlund, R. Alonso-Mori, P. Velikov, D. Wenger, A. Garachtchenko, M. George, V. Borzenets, B. Johnson, T. Rabedeau, and U. Bergmann, "A seven-crystal Johann-type hard x-ray spectrometer at the Stanford Synchrotron Radiation Lightsource," Rev. Sci. Instrum. **84**(5), 053102 (2013).
8. J. Daillant and A. Gibaud, *X-ray and neutron reflectivity-principles and applications* (Springer, 2009), Chap. 3.
9. W. H. Southwell and R. L. Hall, "Rugate filter sidelobe suppression using quintic and rugated quintic matching layers," Appl. Opt. **28**(14), 2949–2951 (1989).
10. P. Baumeister, "Multilayer reflectors with suppressed higher-order reflectance peaks," Appl. Opt. **31**(10), 1568–1573 (1992).
11. B. H. Ibrahim, R. Botha, J. E. Bourée, P. Bulkin, and B. Drévillon, "Correlation of sidelobe suppression between rugate filters and multilayer mirrors," Appl. Opt. **46**(31), 7776–7779 (2007).
12. W. H. Southwell, "Gradient-index antireflection coatings," Opt. Lett. **8**(11), 584–586 (1983).
13. V. Kozhevnikov, I. N. Bukreeva, and E. Ziegler, "Design of x-ray supermirrors," Nucl. Instrum. Methods Phys. Res. A **460**, 424–443 (2001).
14. Y. Yao, H. Kunieda, and Z. Wang, "The theoretical analysis of the hard X-ray block-structure supermirror," Opt. Express **21**(7), 8638–8651 (2013).
15. K. M. M. Prabhu, *Window functions and their applications in signal processing* (CRC, 2013), Chap. 5.
16. K. Yamashita, "Development of Pt/C multilayer supermirrors for hard x-ray optics," Nucl. Instrum. Methods Phys. Res. A **529**(1-3), 59–62 (2004).
17. L. G. Parratt, "Surface studies of solids by total reflection of x-rays," Phys. Rev. **95**(2), 359–369 (1954).
18. Y. Yao, H. Kunieda, H. Matsumoto, K. Tamura, and Y. Miyata, "Design and fabrication of a supermirror with smooth and broad response for hard x-ray telescopes," Appl. Opt. **52**(27), 6824–6833 (2013).
19. F. Schäfers, H. C. Mertins, F. Schmolla, I. Packe, N. N. Salashchenko, and E. A. Shamov, "Cr /sc multilayers for the soft-x-ray range," Appl. Opt. **37**(4), 719–728 (1998).
20. T. Feigl, S. Yulin, N. Benoit, and N. Kaiser, "EUV multilayer optics," Microelectron. Eng. **83**(4–9), 703–706 (2006).
21. D. L. Windt, *IMD version 5.0 installation guide &user's manual* (Reflective X-ray Optics, 2013), Chap. 5.